Periodic states in intermittent pipe flows: Experiment and model

Dimitris Stassinopoulos, Jun Zhang, Preben Alstrøm, and Mogens T. Levinsen
Center for Chaos and Turbulence Studies, Niels Bohr Institute, Ørsted Laboratory, DK-2100 Copenhagen Ø, Denmark
(Received 4 March 1994)

We report an experimental study of a transition to periodic intermittency in pressure-driven pipe flows. The transition is preceded by a rapid increase of the intermittency factor with pressure. To model intermittent pressure-driven flows, we introduce a general model, where a fifth-order Ginzburg-Landau equation is coupled with a pressure-velocity relation that takes into account the frictional effect of the turbulence on the flow velocity. We determine the phase diagram and show that the model gives a qualitative understanding of the transition to periodic intermittency.

PACS number(s): 47.20.−k, 47.27.Cn, 47.27.Eq

I. INTRODUCTION

An intriguing feature of the transition to turbulence is the sudden appearance of turbulent slugs that intermittently break the laminar flow [1–3]. Although slugs usually seem to be generated randomly, periodic generation of slugs are often observed when the flow is pressure driven [3–5]. In this paper we put the production of periodic states under closer scrutiny. We report measurements on the periodic states, which we find to stabilize at intermittency factors [6] γ above 0.6. At lower γ values, signatures of the periodic state are observed in the distribution of laminar lengths. In order to explain the characteristic features observed, including a notable jump in γ vs pressure, we introduce a fifth-order Ginzburg-Landau equation [7,8] coupled with a pressure-velocity relation that takes into account the frictional effect of the turbulence on the flow velocity.

II. EXPERIMENTAL SETUP

The experimental setup is shown in Fig. 1. A cylindrical glass pipe, $d=1$ cm in inner diameter and $L=150$ cm in length, was used. Plastic tubes, 4 cm in inner diameter, connected the pipe to reservoirs. The working fluid was deionized water containing a few drops of homogenized milk whose particles acted as scattering agents (resulting concentration ratio $\approx 10^{-6}$). To remove fluctuations originating from the reservoirs, the inlet section was fitted with tightly packed straws, 9 cm long and 0.5 cm in diameter, and a fly-screen (aperture size = 2.0 mm) was placed 5 cm downstream from the straws and 30.5 cm upstream from the pipe entrance. The axial velocity $V(t)$ in the center of the pipe, 7 cm from the outlet, was measured by laser Doppler velocimetry, using a 15-mW He-Ne laser. The scattered light was detected by a photomultiplier whose output went to a DANTEC 58N20 flow velocity analyzer, where Doppler signals with less than 60 cycles were rejected. The typical sampling rate was about 100 Hz.

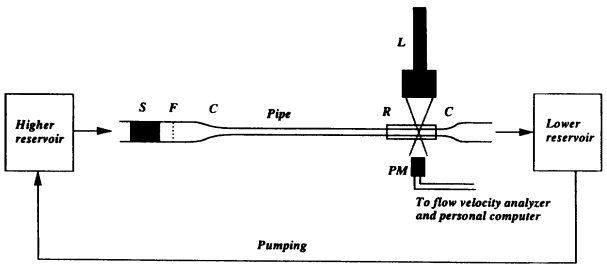

FIG. 1. Schematic illustration of the experimental setup. *S*, straws; *F*, fly screen; *C*, smooth contractions (angle to axial direction $<9°$); *L*, He-Ne laser; *R*, rectangular cell filled with water for elimination of undesirable refraction; PM, photomultiplier.

III. EXPERIMENTAL RESULTS

Two set of experiments were carried out. Due to the smooth contraction section, the onset of turbulence occurred at relatively high Reynolds numbers, $\mathrm{Re}\approx 20\,000$ and 26 000. Here, $\mathrm{Re}\equiv Ud/\nu$, where U is the bulk velocity, and ν is the viscosity of the fluid. In Figs. 2(a) and 2(b) we show the velocity $V(t)$ measured at intermittency factors $\gamma=0.33$ and 0.65. $V(t)$ is observed to alternate between a value $V_{\mathcal{L}}$, where the flow is laminar, and a value $V_{\mathcal{T}}$, where the flow is turbulent [9]. In Fig. 2(b) the alterations in velocity are seen to be essentially periodic. Aside from occasional phase slips [Fig. 2(e)], the periodic states are extremely stable, much longer than the 30-min acquisition time. We estimate the bulk velocity U to be $U_{\mathcal{L}}=0.67V_{\mathcal{L}}$ in the laminar state and $U_{\mathcal{T}}=0.8V_{\mathcal{T}}$ in the turbulent state [10].

The periodic state is only observed at intermittency factors above $\gamma\simeq 0.6$ (inset of Fig. 3). Below this value we observe a rapid increase in γ vs $U_{\mathcal{L}}$. At this transition hybrid states are observed, where the periodic behavior is disrupted by intermittent bursts. For $\gamma=0.35$ the selected laminar time scale can barely be observed as a developing peak in the distribution $p(t_{\mathcal{L}})$ of

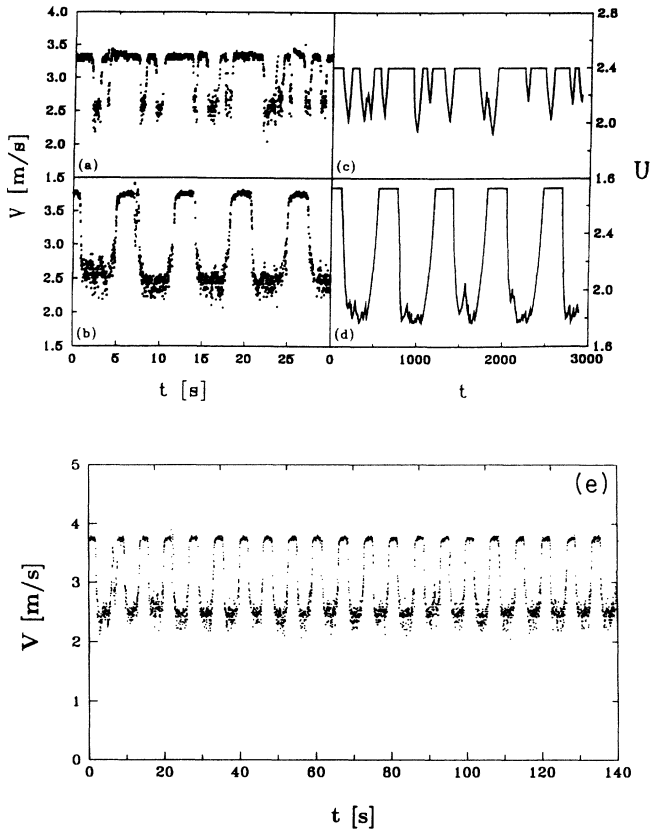

FIG. 2. Left: axial velocity V vs time t, measured at the center and near the outlet: (a) $\gamma=0.33$; (b) $\gamma=0.65$. Right: bulk velocity U vs time t (in units of update-time step) found from simulations of Eq. (1): (c) $\gamma=0.28$; (d) $\gamma=0.57$. Below: (e) periodic intermittency with occasional phase slips; $\gamma=0.65$.

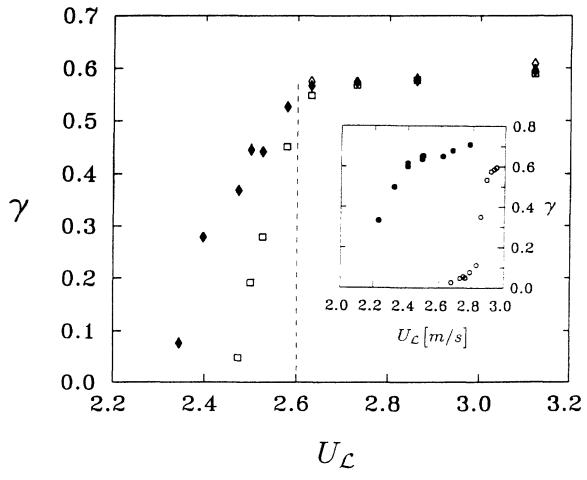

FIG. 3. Intermittency factor γ vs the laminar bulk velocity $U_{\mathcal{L}}$ found from simulations of Eq. (1) with $\sigma=0.077U[t-T(t)]$ and $\mu=-0.0384$. (◇) No noise (γ jumps from 0 to $\gamma_c\simeq 0.6$ at $U_{\mathcal{L}}=U_c=2.60$). (□) Noise $\eta=0.25$. (◇) Noise $\eta=0.5$. Inset: γ vs $U_{\mathcal{L}}$ from experiments; the onset of turbulence is at (●) $U_{\mathcal{L}}=2.0$ m/s, and (○) $U_{\mathcal{L}}=2.65$ m/s.

laminar times [Figs. 4(a)]. By the laminar time $t_{\mathcal{L}}$ (here given in units of the advection time $\tau_{\mathcal{L}}\equiv L/U_{\mathcal{L}}$) we refer to the time it takes for a laminar interval between two slugs to pass the measuring point. In Figs. 4(b) and 4(c) we show the velocity dependence of the mean laminar time $\bar{t}_{\mathcal{L}}/\tau_{\mathcal{L}}$ and the mean turbulent time $\bar{t}_{\mathcal{T}}/\tau_{\mathcal{T}}$ ($\tau_{\mathcal{T}}\equiv L/U_{\mathcal{T}}$). We note that $\bar{t}_{\mathcal{L}}$ diverges at the onset of turbulence; at $U_{\mathcal{L}}=2.0$ m/s and $U_{\mathcal{L}}=2.65$ m/s, respectively. At increasing values of $U_{\mathcal{L}}$, $\bar{t}_{\mathcal{L}}$ makes a dip, then rises to a plateau where $\bar{t}_{\mathcal{L}}\approx 3\tau_{\mathcal{L}}$. The dip signifies the point where the peak starts to develop; at the plateau the peak in $p(t_{\mathcal{L}})$ is very pronounced, corresponding to a periodic state. If we consider $\bar{t}_{\mathcal{T}}$, this is seen to change from $\bar{t}_{\mathcal{T}}\approx\tau_{\mathcal{T}}$, where noise dominates [11], to a plateau at $\bar{t}_{\mathcal{T}}\approx 4\tau_{\mathcal{T}}$, where periodic states are observed.

IV. MODEL

In order to understand qualitatively the one-dimensional nature (spatial scale $\gg d$) of slug production in intermittent pipe flows, we consider a phenomenological fifth-order Ginzburg-Landau model [7,8]

$$\frac{\partial A}{\partial t}=-\frac{\partial V}{\partial A}+\frac{\partial^2 A}{\partial x^2}-U\frac{\partial A}{\partial x}\ , \tag{1a}$$

where $A(x,t)$ is a real function of the position x along the flow and the time t, and

$$V(A,\mu)=-\mu A^2/2-A^4/4+A^6/6\ . \tag{1b}$$

$A(x,t)$ serves as an order parameter for the state of the flow, and the coefficient U represents the bulk velocity of the flow. The boundary conditions are taken to be

$$A(0,t)=\sigma\ ,\quad \frac{\partial A}{\partial x}(L,t)=0\ . \tag{1c}$$

The first boundary condition reflects the assumption that disturbances enter the system and subsequently are advected downstream [8]. The latter boundary condition reflects the fact that the outlet is not a source of disturbance (no reflections, etc.) [12].

The sixth-order form of the potential $V(A)$ models the subcritical nature of the transition to turbulence. The corresponding bifurcation diagram is shown in the inset of Fig. 5. When $\mu<-\frac{1}{4}$, $V(A)$ has a global laminar minimum at $A_{\mathcal{L}}=0$. In the range $-\frac{1}{4}<\mu<0$, $V(A)$ is a three-well potential with local minima at $A_{\mathcal{L}}=0$ and $A_{\mathcal{T}}(\mu)=(\frac{1}{2}+\sqrt{\mu+1/4})^{1/2}$ and a local maximum at $A_1(\mu)=(\frac{1}{2}-\sqrt{\mu+1/4})^{1/2}$. At $\mu=\mu_M=-\frac{3}{16}$, $V(A_{\mathcal{L}})=V(A_{\mathcal{T}})=0$. Only above μ_M will a turbulent slug grow. We shall associate turbulence with a value of the order parameter A larger than a critical value A_c, chosen to be $A_c=A_{\mathcal{T}}(-\frac{1}{4})=1/\sqrt{2}$. Otherwise the flow will be considered laminar. Figure 5 shows the first phase diagram obtained for Eq. (1) [$L>100$]. For every value of σ there is a tongue separating the laminar state from the turbulent state (laminar below the tongue). At large velocities the transition between laminar and turbulent flow is

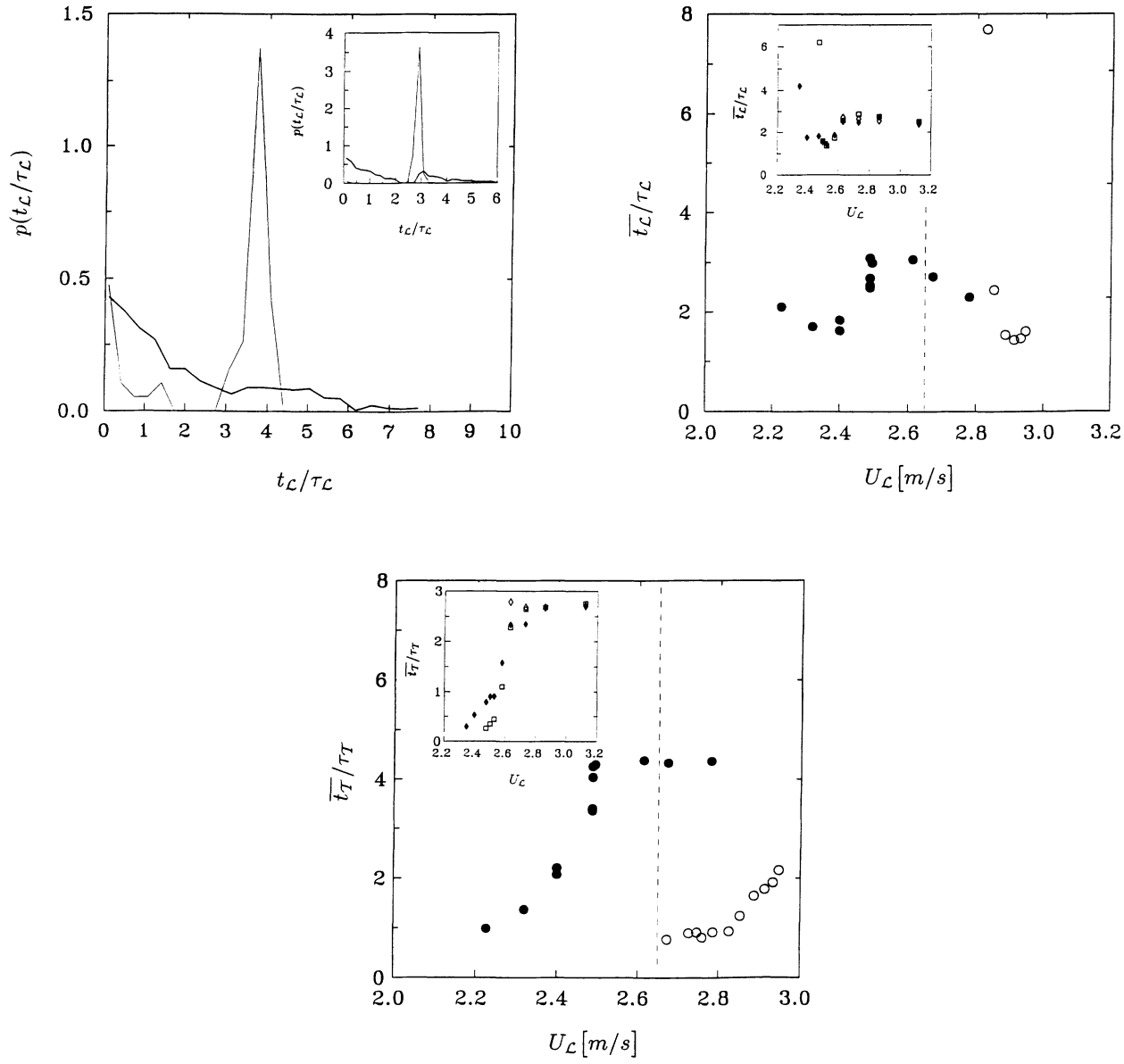

FIG. 4. (a) Distributions of laminar times for $\gamma=0.35$ (thick line) and 0.65 (thin line). (b) Mean laminar and (c) mean turbulent times vs the laminar bulk velocity U_L. Symbols as in the inset of Fig. 3. Insets: corresponding results obtained from simulations of Eq. (1) with $\sigma=0.077U\,[t-T(t)]$ and $\mu=-0.0384$. (a) $\gamma=0.28$ (thick line) and 0.57 (thin line). (b) and (c) Symbols as in Fig. 3. In the case of no noise, $\bar{t}_L$ jumps to infinity at $U_L=U_c=2.60$.

given by $A_1(\mu)=\sigma$, but at lower velocities a hysteretic regime exists [8], where the selected state depends on the history. Also shown in Fig. 5 is the line separating the convective flow from the absolute unstable flow.

To model pressure-driven pipe flows, we must take into account that the bulk velocity decreases when the fraction f_T of turbulence in the pipe increases, due to larger friction. More precisely, Eq. (1) must be coupled with a relation [13] $U=U(G,f_T)$, where G is the dimensionless pressure gradient [14] $G\equiv gd^3\Delta h/\nu^2 L$. This pressure-velocity relation is essential for the formation of periodic states. The total pressure drop is the sum of the pressure drop over the laminar part and the pressure drop over the turbulent part of the flow. We assume that $U(G,f_T)$ is implicitly given by

$$G=f_L a_L \mathrm{Re}^{b_L}+f_T a_T \mathrm{Re}^{b_T}\ , \tag{2}$$

where $f_L=1-f_T$. In terms of the order parameter A, the fraction of turbulence in the pipe is

$$f_T(t)=\int_0^L \theta(A(x,t)-A_c)dx/L\ , \tag{3}$$

where θ is the theta function. The parameters a_L and b_L

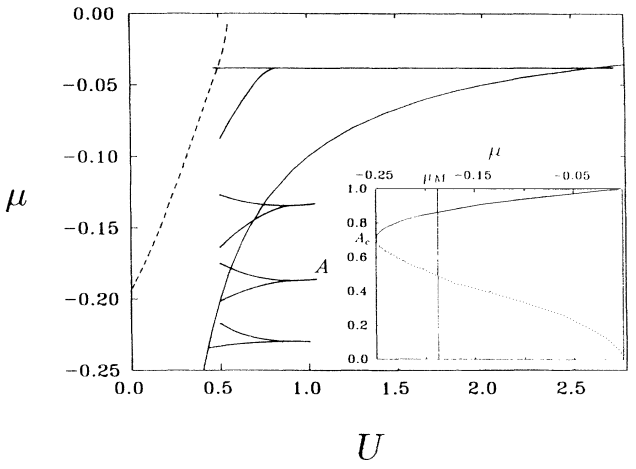

FIG. 5. Phase diagram for Eq. (1) at large L. The tongues separating the laminar from the turbulent flow are shown for $\sigma=0.2$, 0.4, 0.5, and 0.6 (from top to bottom). The dashed line is the transition line between the convective and the absolute unstable flows. Also shown is the curve $\mu(U)=-0.1U^{-1}$. Inset: bifurcation diagram for Eq. (1).

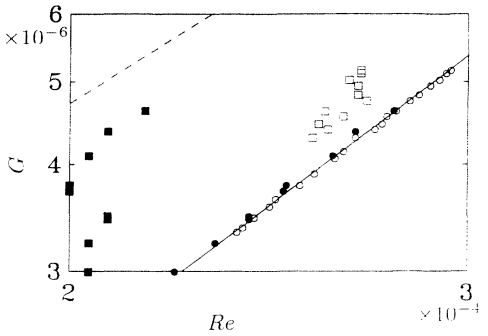

FIG. 6. Double-logarithmic plot of dimensionless pressure gradient G vs Reynolds number Re. In the intermittent regime, Re alternates between a laminar value (circles) and a turbulent value (squares). The onset of turbulence occurs at $\mathrm{Re}\approx 20\,000$ (filled symbols) and $\mathrm{Re}\approx 26\,000$ (open symbols). The laminar values follow a quadratic fit, $G=0.006\mathrm{Re}^2$ (solid line). Above our data is shown the line assumed for the fully turbulent flow, $G=0.32\ \mathrm{Re}^{5/3}$ (dashed line).

for the fully laminar flow ($f_{\mathcal{L}}=1$) were determined experimentally to be $a_{\mathcal{L}}=0.006$ and $b_{\mathcal{L}}=2$ (Fig. 6). For the fully turbulent flow ($f_{\mathcal{T}}=1$), we use the parameters $a_{\mathcal{T}}=0.32$ and $b_{\mathcal{T}}=\frac{5}{3}$ found from Refs. [3] and [15].

V. NUMERICAL RESULTS AND COMPARISON WITH EXPERIMENTS

In our simulations of Eqs. (1) and (2), L is taken to be 256, and the Reynolds number in Eq. (2) is replaced by $5000U$ (see below). The flow is more stable at lower velocities. Since σ represents the disturbance at the entrance, and μ is the instability parameter, we thus expect both to increase with velocity. Furthermore, μ is in general a function of the spatial coordinate x as well. Here we consider either μ or σ (but not both) as an increasing function of the velocity. In either case we find a strict periodic behavior. We shall see that the exact form of these two functions does not affect the physics in a significant way. Moreover, in general accordance with experiment, we find that the front and rear of a developed slug are sharp (width ≈ 5) and move independently; their velocities depend only on the velocity U.

Consider the case $\sigma=0.2$ and $\mu(U)=-0.1U^{-1}$ (well inside the convective unstable regime; see Fig. 5). Our constraint $U(\mathrm{Re}=5000)=1$ implies that $\mu(\mathrm{Re}=2000)=-\frac{1}{4}$, which expresses the observation that no turbulence is sustainable below $\mathrm{Re}\approx 2000$ [1–3]. The onset of turbulence is found at $\mu(U)=-0.0384[A_1(\mu)=0.2]$, hence at $U=U_c=2.60$, corresponding to a Reynolds number $\mathrm{Re}=13\,000$. The key element in sustaining a periodic cycle lies in the consistency with which the flow rate moves above ($A_{\mathcal{T}}$ stable) and below ($A_{\mathcal{L}}$ stable) the critical velocity U_c. The periodic state is dominated by the advection time $\tau_c\equiv L/U_c\simeq 100$. A universal feature of the transition to periodic intermittency is an abrupt jump in the intermittency factor γ (determined at $x=L$). In the present case we find that γ jumps to a value $\gamma_c\simeq 0.4$. In most cases of interest, however, the constant disturbance σ plays the role of the zero-order Fourier component of a noisy signal; superimposing random fluctuations, the jump is smooth. However, to observe periodic states the scatter $\delta\mu$ in μ imposed by the noise, $A_1(\mu\pm\delta\mu)=\sigma(1\mp\eta)$, must be smaller than the change $\mu(U_{\mathcal{L}})-\mu(U_{\mathcal{T}})$ due to friction. Experimentally, this translates into a restriction on the critical Reynolds number for a given pipe length.

Next, consider the case $\sigma(U)=0.077U$ and $\mu=-0.0384$. The onset of turbulence is at $U_c=2.60$ ($\sigma=0.2$) as before. Not surprisingly, we find essentially the same results. However, a difference between model and experiment is found: experimentally, the period is longer than the advection time. The difference indicates that the primary source of disturbance lies behind the pipe entrance ($x=0$). However, these disturbances first affect the flow when entering the pipe. To simulate the time delay we assume that σ is a retarded function of U, $\sigma=0.077U\,[t-T(t)]$, where $T(t)$ is the time it takes a fluid element to travel from the source of disturbance to the pipe entrance, i.e., $\int_{t-T(t)}^{t}U(\tau)d\tau=L_0$, where L_0 is a geometry-dependent constant (L_0 depends on the form of the contraction section) [16]. We have simulated Eqs. (1) and (2) with the retarded boundary condition, taking $L_0=2L$. We find that the value of the intermittency factor at the transition to periodic intermittency is larger than before ($\gamma_c\simeq 0.6$), and the emergence of a plateau following the jump is consistent with experiments (Fig. 3). Adding noise allows us to make a closer comparison with experiment. We therefore consider the situation where $A(0,t)$ at every time step $\Delta t\equiv 1/U$ is chosen from a uniform distribution between $(1-\eta)\sigma(U[t-T(t)])$ and $(1+\eta)\sigma(U[t-T(t)])$. The resulting behavior of the in-

termittency factor is shown in Fig. 3 for $\eta=0.25$ and 0.5; the jump in γ becomes steeper at lower values of η. Accordingly we find a steeper jump in γ for the high-Re experiment.

In Figs. 2(c) and 2(d) the bulk velocity $U(t)$ obtained for $\eta=0.5$ is shown at intermittency factors $\gamma=0.28$ and 0.57. In accordance with experiments, a clean periodic behavior is seen at high γ values [Fig. 2(d)], while noise dominates at low-γ values [Fig. 2(c)]. When γ is not too low, the laminar time scale gives rise to a peak in the distribution $p(t_{\mathcal{L}})$ of laminar times [inset of Fig. 4(a)]. In the inset of Figs. 4(b) and 4(c), we show the velocity dependence obtained for the mean laminar time $\bar{t}_{\mathcal{L}}$ and the mean turbulent time $\bar{t}_{\mathcal{T}}$ in units of the advection times $\tau_{\mathcal{L}}$ and $\tau_{\mathcal{T}}$. In qualitative agreement with experiment, $\bar{t}_{\mathcal{L}}$ has a dip before rising to a plateau, signifying the onset of periodic intermittency. The value of $\bar{t}_{\mathcal{L}}$ at this plateau depends on the choice of L_0; here $\bar{t}_{\mathcal{L}}\approx 3\tau_{\mathcal{L}}$. The qualitative behavior of $\bar{t}_{\mathcal{T}}$ also agrees with experiment. It changes abruptly from a noise dominated regime where $\bar{t}_{\mathcal{T}}\approx\tau_{\mathcal{T}}$ to a plateau at $\bar{t}_{\mathcal{T}}\approx 3\tau_{\mathcal{T}}$, where clear periodic states are observed.

VI. CONCLUSION

In summary, we have introduced a general model for intermittent pressure-driven pipe flows that reproduce qualitatively the characteristic features found at the onset of periodic intermittency. However, the model can be applied to explain other features as well. One of them is the puffs found at $\mathrm{Re}\approx 2500$ [2]. These are stable turbulent droplets that do not grow. In our phase diagram (Fig. 5) this corresponds to a value $\mu\approx\mu_M$. A slug formed above but near $\mu=\mu_M$ will only spread until $\mu=\mu_M$, and then stabilize as a turbulent puff.

ACKNOWLEDGMENT

This work was supported by the Novo-Nordisk Foundation and the EC Science plan.

[1] O. Reynolds, Philos. Trans. R. Soc. London, Ser. A **186**, 123 (1895).

[2] I. J. Wygnanski and F. H. Champagne, J. Fluid Mech. **59**, 281 (1973).

[3] D. J. Tritton, *Physical Fluid Dynamics* (Oxford Science Publications, Oxford, 1988).

[4] P. V. Pantulu, M. S. thesis, Department of Aeronautical Engineering, Indian Institute of Science, Bangalore, 1962.

[5] K. R. Sreenivasan and R. Ramshankar, Physica D **23**, 246 (1986).

[6] γ is the fraction of time the flow is turbulent at the measuring point.

[7] Y. Pomeau, Physica D **23**, 3 (1986); R. J. Dreissler, Phys. Lett. A **120**, 334 (1987); O. Thual and S. Fauve, J. Phys. (Paris) **49**, 1829 (1988). The dynamics considered happens on time and space scales longer than those relevant for the vortex dynamics (those emerging from possible complex terms are here integrated out).

[8] J. M. Chomaz, Phys. Rev. Lett. **69**, 1931 (1992).

[9] $V_{\mathcal{L}}$ and $V_{\mathcal{T}}$ were found as peak values in the velocity distribution. The scatter in $V_{\mathcal{L}}$ was 1%, in $V_{\mathcal{T}}$ it was 15%.

[10] The ratio $U_{\mathcal{L}}/V_{\mathcal{L}}=0.67$ at the pipe outlet is derived from the velocity profile given by E. M. Sparrow, S. H. Lin, and T. S. Lundgren, Phys. Fluids **7**, 338 (1964). These profiles are in good agreement with those we find experimentally. The ratio $U_{\mathcal{T}}/V_{\mathcal{T}}=0.8$ is found from the condition that $U_{\mathcal{T}}\simeq U_{\mathcal{L}}$ at the onset of turbulence, where the fraction $f_{\mathcal{T}}$ of turbulence in the pipe is small.

[11] J. Zhang, D. Stassinopoulos, P. Alstrøm, and M. T. Levinsen, Phys. Fluids **6**, 1722 (1994).

[12] The first derivative is sometimes replaced by the second derivative. In the present studies, where the pipe length substantially exceeds the front widths, it plays no role which one of the derivatives is chosen.

[13] The inertia of the fluid is neglected in order to write $U(t)$ as a function of G and $f_{\mathcal{T}}$ only.

[14] Δh is the height difference between the water levels of the two reservoirs; g is gravity.

[15] From Eq. (2) the fraction $f_{\mathcal{T}}$ of turbulence in the pipe can be estimated from our data for U_L and U_T. Our largest value of $f_{\mathcal{T}}$ estimated this way is found to be ≈ 0.7. By direct measurements at different points downstream, we find the same result.

[16] $L_0\equiv d^{-2}\int_{-L_f}^{0}[d(x)]^2dx$, where L_f is the actual distance from the source of disturbance to the pipe entrance, and $d(x)$ is the diameter of the inlet section at a distance x. For example, if $L_f=30.5$ cm (distance to fly screen), we find $L_0\approx 400\ \mathrm{cm}\simeq 2.7L$.

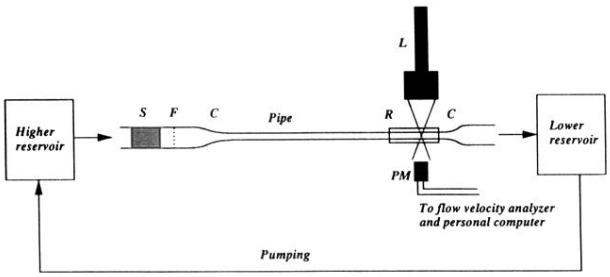

FIG. 1. Schematic illustration of the experimental setup. *S*, straws; *F*, fly screen; *C*, smooth contractions (angle to axial direction $<9°$); *L*, He-Ne laser; *R*, rectangular cell filled with water for elimination of undesirable refraction; PM, photomultiplier.